■ ANNOTATION

Effects of titanium nanotubes on the osseointegration, cell differentiation, mineralisation and antibacterial properties of orthopaedic implant surfaces

E. P. Su,
D. F. Justin,
C. R. Pratt,
V. K. Sarin,
V. S. Nguyen,
S. Oh,
S. Jin

From Nanovation Partners, LLC, Camarillo, California, United States

The development and pre-clinical evaluation of nano-texturised, biomimetic, surfaces of titanium (Ti) implants treated with titanium dioxide (TiO_2) nanotube arrays is reviewed. *In vitro* and *in vivo* evaluations show that TiO_2 nanotubes on Ti surfaces positively affect the osseointegration, cell differentiation, mineralisation, and anti-microbial properties. This surface treatment can be superimposed onto existing macro and micro porous Ti implants creating a surface texture that also interacts with cells at the nano level. Histology and mechanical pull-out testing of specimens in rabbits indicate that TiO_2 nanotubes improves bone bonding nine-fold (p = 0.008). The rate of mineralisation associated with TiO_2 nanotube surfaces is about three times that of non-treated Ti surfaces. In addition to improved osseointegration properties, TiO_2 nanotubes reduce the initial adhesion and colonisation of *Staphylococcus epidermidis*. Collectively, the properties of Ti implant surfaces enhanced with TiO_2 nanotubes show great promise.

Cite this article: *Bone Joint J* 2018;100-B(1 Supple A):9–16.

■ E. P. Su, MD, Associate Professor of Clinical Orthopaedics, Weill Cornell Medical College, New York, NY, USA and Associate Attending Orthopaedic Surgeon, Adult Reconstruction and Joint Replacement Division Hospital for Special Surgery, New York, USA.

■ D. F. Justin, MS, President and CEO
■ C. R. Pratt, JD, Chairman
■ S. Jin, PhD, Chief Scientific Advisor
Nanovation Partners, LLC, Camarillo, California, USA.

■ V. K. Sarin, PhD, President Kinamed Incorporated, Camarillo, California, USA

■ V. S. Nguyen, MD, Chairman Optimotion Implants, LLC, Orlando, Florida, USA.

■ S. Oh, PhD, Professor Department of Dental Biomaterials, College of Dentistry, Wonkwang University, Iksan, Jeonbuk, Republic of Korea.

Correspondence should be sent to D. F. Justin; email: danj@nanovationpartners.com

doi:10.1302/0301-620X.100B1.BJJ-2017-0551.R1 $2.00

Bone Joint J 2018;(1 Supple A):9–16.

Titanium (Ti) and its alloys have been widely used in orthopaedic implants for decades, due to their biocompatibility, low toxicity, and excellent mechanical properties.[1] When designed with macro porous and micro-textured features for enhanced osseointegration, implants made from Ti alloys bond with adjacent bone surfaces relatively well compared with those made from other materials with similar macro and micro features. However, complications such as aseptic loosening and infection persist.[2-4] Inadequate osseointegration remains a complication associated with implants that rely on osseointegration for proper function, particularly those with relatively flat and small surface areas that have high shear loading, such as non-cemented uni and total condylar knee tibial trays.[5,6] Faster osseointegration can enhance recovery as a result of improved load distribution and a more stable bone-implant interface.

Over the past six decades, the surface technologies of implants have progressed from bioinert surfaces such as porous Ti and tantalum, to bioactive surfaces such as plasma-sprayed hydroxyapatite and other ceramics, to the most recent and probable future generation of biomimetic engineered, nano-texturised surfaces such as Ti treated with Ti oxide (TiO_2) nanotube arrays. These surfaces mimic the nano-morphology of the external cellular membranes of the osteoblasts that surround the implant. A substantially increased surface area has unique chemical characteristics provided by the nanotubes, allowing increased interaction between the surface of the implant and adjacent cells. Nano-surface mechanisms increase the rate of initial osseointegration between Ti alloys and the surrounding tissue, greatly increasing the strength of the bond between implant and bone.[7]

Nano-technology is the control of matter at a scale of approximately 1 to 100 nanometres (nm), where novel properties and function occur because of size.[8] Thus, for the surface of an implant truly to possess nano-technology, aspects of shape and structure must be formed at the nano-scale which specifically enhance the properties of the implant. The impact that nano-texturising has on the interactions of the surface of the implant can be illustrated by imagining the macro, micro, and nano-surface area of a 1 cm × 1 cm × 1 cm cubic implant, which has 6 cm^2 of macro surface area (about the size of a sugar cube), as shown in Figure 1.[8] If such an implant is divided into 1 mm cubes, the total surface area increases to 60 cm^2. If it is further divided into 1 nm cubes, the surface area increases to 60 000 000 cm^2, equivalent to approximately 1.5 acres of surface area. Likewise, nano-texturing an implant with features such as tubes that have both internal and external surface areas greatly increases the area

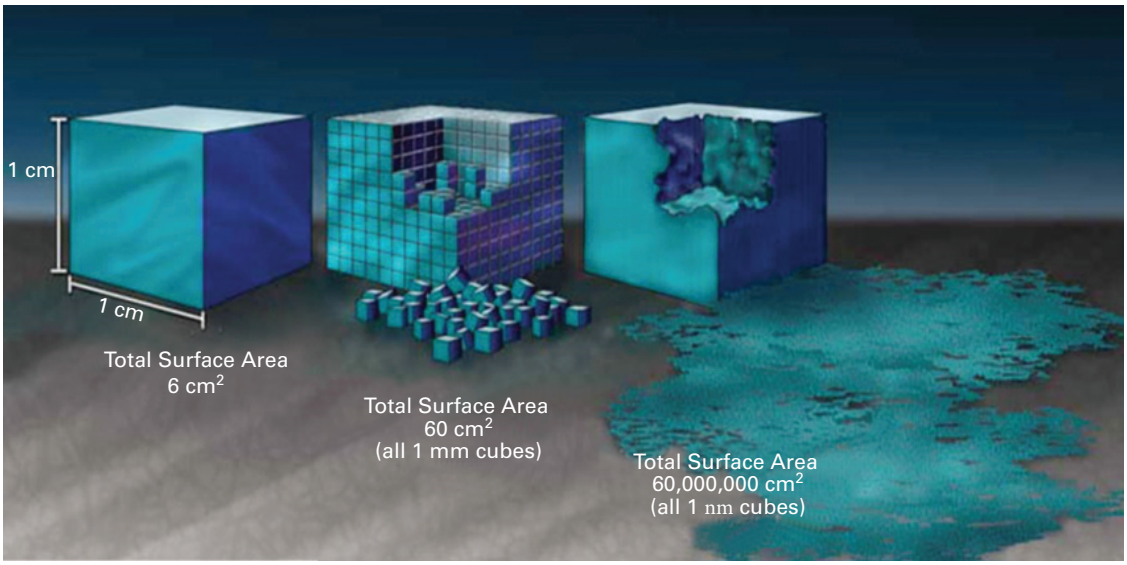

Fig. 1

Graphic illustration of the increased surface area provided by nano-texturising. Adapted with permission from the National Nanotechnology Coordination Office ITRI, Inc.[8]

available for osseointegration between the nano-scale features of the tubes and those of the cells.

TiO_2 nanotube arrays are formed on Ti surfaces through a specialised efficient anodisation process that is followed by heat treatment.[9-14] The arrays consist of rows of vertically aligned nanotubes with engineered and reproducible internal diameters, outer diameters, and lengths, resulting in a nano-textured surface of nanotubes that has defined, non-random physical and chemical properties. In order to treat a Ti implant, it is first immersed in a fluoride-rich electrolyte. As a voltage is applied, a thicker compact layer of TiO_2 develops on the outer surface. Then, during an extended anodisation process of approximately ten minutes to 45 minutes, depending on the volume and surface area of the implant, billions of vertically aligned nanotubes are integrated into the outer TiO_2 layer, creating a surface of nano-texturised TiO_2 nanotubes. After anodisation, the surface is heat treated to 500°C for two hours to convert the TiO_2 nanotubes from an amorphous phase to an anatase phase. This post-anodisation heat treatment improves both the toughness of the nanotubes and their osseointegration potential.[15] The resultant surface is not a coating but a transformed TiO_2 surface, which not only greatly increases the available surface area for processes such as cell adhesion, but also provides a nano-texture that interacts with outer cell membrane surfaces. Such TiO_2 nano-texturised surfaces exhibit tensile and shear adhesion strengths that exceed the typical loads experienced during the introduction of implants, their use and their removal.[16]

The anodisation process can be adjusted to create nano-texturised surfaces of vertically aligned nanotubes with accurately controlled pore diameters. For example, specimens can be made with a mean outside diameter of the nanotube of 30 nm (SD 10 nm), 70 nm (SD 10 nm), or 100 nm (SD 10 nm), and with specific thicknesses and heights of the walls. A nano-texturised surface with a mean diameter of the nanotube of 100 nm has a high hydrophilicity when compared with a non-nano-texturised Ti surface or a nano-texturised surface with a mean diameter of 30 nm.[17,18] The hydrophilicity of the surface of a nanotube array is inversely related to the diameter of the tube. The higher the hydrophilicity, the more absorbent the surface and the smaller the contact angle surrounding liquid on the surface.[17,18] The formation of vertically aligned TiO_2 nanotubes on the surface of a Ti implant can positively affect the osseointegration, cell differentiation, mineralisation, and antimicrobial properties. Figure 2 shows an example of a tibial tray that incorporates macro features, micro porosity, and nano-texturing to enhance fixation.

We present a review of recent research to summarise the outcomes that can be achieved by the creation of vertically aligned TiO_2 nanotubes on a Ti implant surface.

Osseointegration and cell differentiation

Oh et al[15,19] studied the *in vitro* behaviour of osteoblasts cultured on vertically aligned TiO_2 nanotubes and investigated the effect of such a nano-structure on the morphology of osteoblasts and the kinetics of cell proliferation. A layer of vertically aligned TiO_2 nanotubes on a Ti surface was created by anodisation, and MC3T3-E1 mouse osteoblast cells were seeded on the experimental substrate and on a control substrate of pure non-texturised Ti. The presence of nanotubes positively affected the adhesion and propagation of the osteoblasts, with the filopodia of the growing cells spreading across the pores of the nanotube arrays, producing an interlocked cell structure. With the passage of time,

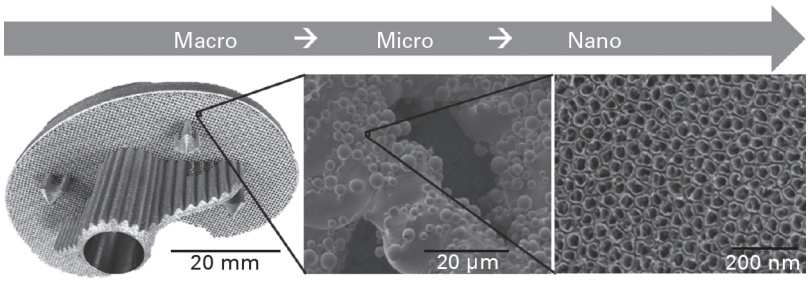

Fig. 2

Titanium alloy tibial tray incorporating macro fixation with pegs and keels; micro fixation with additive manufactured micrometer scale porosity, and nano-scale texturing throughout the porosity with anodised titanium dioxide nanotubes. Image courtesy of Optimotion Implants, LLC, Orlando, Florida. Macro (mm scale); Micro (µm scale); Nano (nm scale).

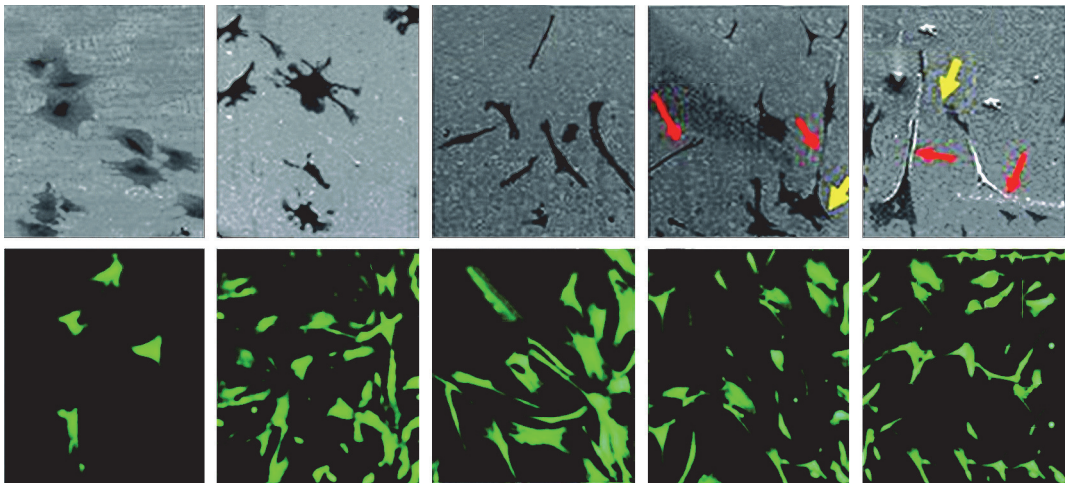

Fig. 3

Mesenchymal stem cells at 24 hours. Upper row (left to right): scanning electron microscope micrographs of human mesenchymal stem cells (hMSCs) on flat Ti and 30 nm, 50 nm, 70 nm and 100 nm diameter Ti dioxide (TiO_2) nanotube surfaces after two hours of culture. Lower row (left to right): fluorescent images of hMSCs on flat Ti and 30 nm, 50 nm, 70 nm, and 100 nm diameter TiO_2 nanotube surfaces showing increase in cell elongation with increasing nanotube diameter.

the number of adhered cells on the TiO_2 nanotubes increased significantly by approximately 300% to 400% compared with the number of cells adhering to the Ti metal surface. This effect is most likely to be due to the increased surface area, the increased hydrophilicity, and the unique topography of nanotubes that increases the negative charge on the outer rim of the tubes.[19]

Gongadze et al[20] have suggested that the attraction between the negatively charged Ti surface and a negatively charged osteoblast is mediated by charged proteins with a distinctive distribution of quadrupolar internal charge. Similarly, cation-mediated attraction between fibronectin molecules and the Ti surface is expected to be more efficient for a high surface charge density, resulting in integrin mediated osteoblast adhesion. The osteoblasts are most strongly bound along the sharp convex edges of the surfaces of the TiO_2 nanotube where the magnitude of the density of the negative surface charge is the highest. A vertically aligned nanotube configuration may be a useful route for accelerating the proliferation of various other types of cells in addition to osteoblasts.[17]

As described above, the pore diameter of TiO_2 nanotubes can be controlled by adjusting the potential during anodisation. In an *in vitro* examination of human mesenchymal stem cells (hMSC), Oh et al[15] created TiO_2 nanotubes with pore diameters ranging from 30 nm to 100 nm. Varying the pore diameters of nano-tubular-shaped TiO_2 surface structures independently allowed either augmented hMSC adhesion or a specific differentiation of hMSCs into osteoblasts by using only the geometric cues, without the introduction of osteogenic-inducing media. The behaviour of hMSC in response to the varied sizes of nanotubes revealed a significant change in a relatively narrow range of sizes. As shown in Figure 3, small (~30 nm diameter) nanotubes promoted adhesion without noticeable differentiation, whereas larger (~70 nm to 100 nm diameter) nanotubes elicited a dramatic elongation of stem cells (~10-fold increase), which induced cytoskeletal stress and selective differentiation into osteoblast-like cells.

Similarly, osteoblasts can exhibit increased elongation when cultured on TiO_2 nanotubes of increasing diameter.

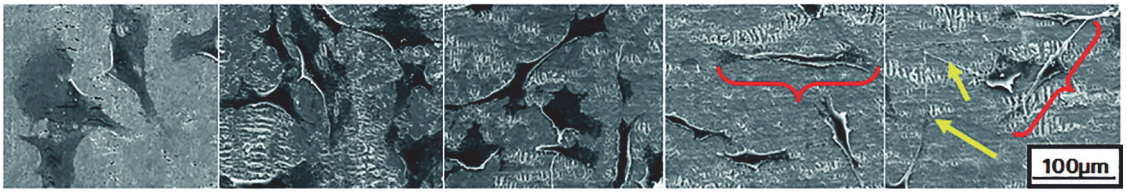

Fig. 4

Scanning electron microscope micrographs of osteoblasts (which appear dark) on (left to right) flat titanium (Ti) and 30 nm, 50 nm, 70 nm, 100 nm diameter Ti dioxide (TiO_2) nanotube surfaces after 24 hours of incubation. The arrows indicate strikingly long cellular extensions across the substrate on the 100 nm nanotubes. Red brackets show increased cellular elongation on the larger ~70 nm to 100 nm diameter nanotubes. Flat and more rounded cells are shown on Ti and 30 nm to 50 nm TiO_2 nanotube surfaces.

Brammer[18] prepared TiO_2 nanotubes of 30 nm, 50 nm, 70 nm and 100 nm pore diameter on Ti substrates by anodisation, and seeded the substrates with MC3T3-E1 mouse osteoblasts to investigate cellular behaviour in response to the different sizes of nanotube. They observed that a change in osteoblast behaviour was obtained in a relatively narrow range of nanotube dimensions; those with a small diameter (~30 nm) stimulated the highest degree of osteoblast adhesion, while those with a larger diameter (70 nm to 100 nm) stimulated a lower population of cells with extremely elongated cellular morphology and much higher levels of alkaline phosphatase, as shown in Figure 4. Increased elongation of nuclei is also seen with larger diameter nanotubes.[18]

The rate of cell adhesion may be significantly increased on nano-textured surfaces. Peng et al[21] found, in an *in vitro* study comparing the cellular response with different textured surfaces, that the adhesion of C3H10T1/2 mouse cells on the surface of Ti specimens treated with TiO_2 nanotube arrays, 30 nm or 80 nm in diameter, was significantly enhanced when compared with control samples cultured on polished Ti and acid-etched Ti. A surface analysis of the four groups (group one, polished Ti; group two, acid etched Ti; group three, nanotubes with a mean diameter of 80 nm; and group four, nanotubes with a mean diameter of 30 nm) identified increased surface roughness, decreased water contact angles and an enhanced concentration of oxygen and fluorine atoms on the surfaces of TiO_2 nanotubes. The density on the 30 nm and 80 nm TiO_2 nanotube arrays was found to be higher than that on the mechanically polished and acid-etched Ti sheets ($p < 0.01$), and the cell density on the 80 nm TiO_2 nanotube arrays was markedly higher than that of the other groups at two, eight, 12, and 24 hours. The authors concluded that the surface of a TiO_2 nanotube can reduce bacterial colonisation (as described below) and enhance C3H10T1/2 cell adhesion. Many physical and chemical properties of the surface of a TiO_2 nanotube may contribute to these effects.

Adhesion strength, or implant-bone bonding, was measured in an *in vivo* study comparing the surface of a TiO_2 nanotube implant with the surface of a Ti grit-blasted implant. Bjursten et al[7] implanted discs with TiO_2 nanotube surfaces and control discs with Ti grit-blasted surfaces in compression on the flat cortical bone non-load-bearing surface of the proximal anterior tibias of rabbits. Weight-bearing was allowed immediately following surgery. The grit blasted surfaces had a micro-surface roughness with features approximately 6 µm long by approximately 2 µm deep and an outer layer of approximately 5 nm of amorphous TiO_2. The TiO_2 nanotube treated implants had an approximately 250 nm to 300 nm thick layer of anatase TiO_2 nanotubes that were 100 nm outer diameter by 80 nm inner diameter formed by anodisation. After removing the tibial periosteum in the area of attachment of the implant, and reaming the exposed bone surface flat with a circular reamer, the implants were held in compression by Teflon (DuPont Co., Wilmington, Delaware) coverings that were installed over the disc-shaped implants to hold them securely.

After four weeks, the coverings were removed, and screws were attached to the discs in harvested necropsy samples and pulled slowly at 0.1 mm/sec to measure adhesion strength in pure tension. Pull-out testing indicated that the strength of bonding of the TiO_2 nanotubes improved by nine-fold ($p = 0.008$) compared with the blasted micro-textured surface (mean 10.8 N (SD 3.1 N) *vs* mean 1.2 N (SD 2.7 N)), as shown in Figure 5. Furthermore, the TiO_2 nanotube implants showed significantly higher bone-implant contact area (mean 78.3% (SD 33.3)) compared with the micro-textured implants (mean 21.7% (SD 24.7)). Histological analysis, illustrated in Figure 6, confirmed greater bone-implant contact area, new bone formation and increased levels of calcium and phosphorus on the surfaces of the nanotubes compared with the micro-textured implants. Energy dispersive radiograph mapping of the interface after tensile testing indicated a higher surface area and increased calcium and phosphorus on the TiO_2 nanotube surfaces compared with the blasted implant surfaces. The percentage of surface area covered by calcium and phosphorous, which is indicative of strong osseointegration, was approximately 41.7% on TiO_2 nanotube surfaces *versus* only 8.3% for the micro-textured surfaces. The bond between newly formed bone and the surfaces of the TiO_2

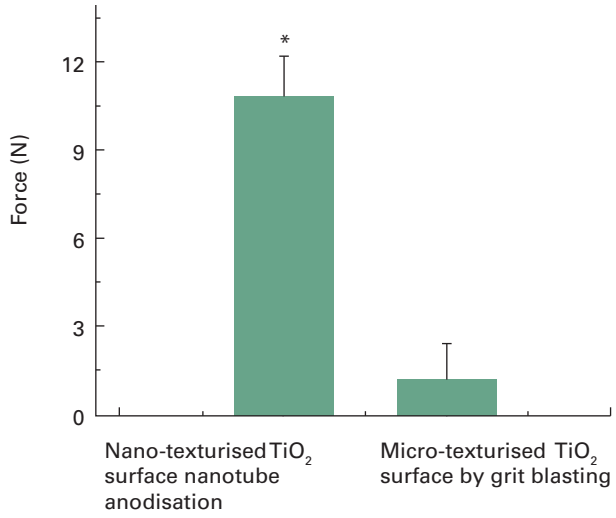

Fig. 5

Results of tensile pull-out tests for titanium dioxide (TiO_2) nanotube *versus* TiO_2 micro-texturised, grit blasted disk implants (*p-value = 0.008).

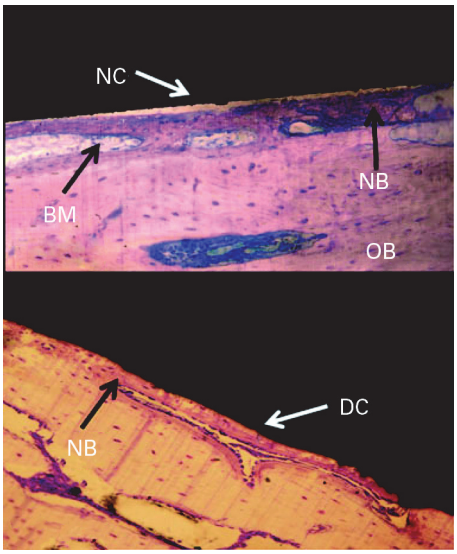

Fig. 6

Haematoxylin and eosin stained ground sections with thickness of 25 µm to 50 µm showing direct contact (DC) or non-direct contact (NC) with bone on (top) titanium (Ti) micro-texturised grit blasted implant and (bottom) Ti dioxide nano-texturised nanotube implant. Bone marrow (BM), old bone (OB), and new bone (NB) are indicated.

nanotubes was so strong that fracture occurred within the growing bone rather than at the implant-bone interface.

A nano-surfaced material in the range below 100 nm more closely mimics the natural hydroxyapatite and collagen constituents of bone than a micro-scale textured surface alone. The nano-topography of the TiO_2 nanotubes more closely resembles the porous structure of native bone, allowing for more optimal interactions for osteogenesis.[7] As protein adsorption on the surface occurs first on implantation, the nanotubes provide a more favourable structure to attract proteins, such as vitronectin and fibronectin, which promote the adhesion of osteoblasts onto the surface of the implant. Nanotubes improve adhesion and proliferation for osteoblasts through their improved focal adhesion.[15] Thus, one of the major benefits of nano-surfacing seems to be the initial enhancement of osteoblast attachment and accelerated osseointegration. When sufficient time is allowed without micro-movement between the implant and bone, an implant surface without nanostructure eventually seems to catch up, although at a slower rate, and produces a comparable degree of bone formation with a nano-textured surface. However, the quality of osseointegration and bone bonding may still not match that of a nano-textured surface.

Ti nanotubes may also be formed on Ti coatings applied to cobalt chrome (CoCr) implants. Figure 7 shows *in vitro* osteoblast formation on a CoCr implant with a Ti coating and TiO_2 nanotubes after 24 hours.[22] Similar to TiO_2 nanotubes on solid Ti implants, the osteoblasts are elongated, with prominent filopodia. These results are like the results seen in Figure 4 (osteoblast cells on TiO_2 nanotubes on a Ti implant). In addition, the cells may show large focal adhesions, which are vital for proper cell function.

Mineralisation

Bone mineralisation occurs when an inorganic substance, such as calcium or phosphorus, precipitates in an organic matrix such as an osteoblast. As reported by Frandsen et al,[22] TiO_2 surfaces with Ti nanotubes show an increased rate of mineralisation compared with a pure Ti surface. In this *in vitro* study, the behaviour of human osteoblast cells on TiO_2 nanotubes and tantalum (Ta) coated TiO_2 nanotube surfaces of nearly identical nano-topography were compared to assess the effect of changes in surface characteristics due to a Ta coating alone. Although the rate of mineralisation of the surface of a TiO_2 nanotube array is about three times faster than that of Ti micro-textured by blasting, and about twice as fast as micro-textured Ta, the rate can be further enhanced by adding nano-particles of Ta to the nanotubes. The 'osteofunctionality' was enhanced on the Ta surface as measured by alkaline phosphatase activity, bone nodule formation, and the deposition of matrix minerals. The Ta surface promoted an approximately 30% faster rate of mineralisation and bone-nodule formation compared with the results on bare TiO_2 nanotubes. Table I and Figure 8 compare the rates of mineralisation for phosphorus and calcium on Ti and Ta substrates, on TiO_2 surfaces with Ti nanotubes and on Ti nanotubes further enhanced with a Ta nano-particle coating. The Ta enhanced nanotubes provide an almost four-fold increase in the rate compared with the micro-texturised Ti surfaces used in

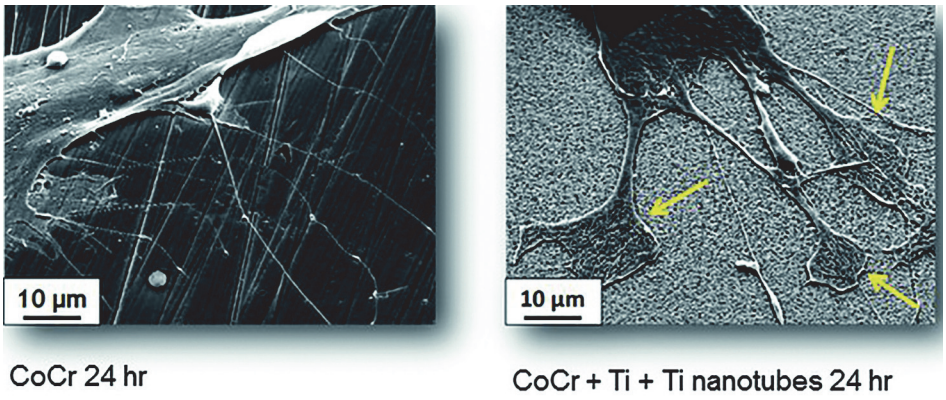

Fig. 7

Scanning electron microscope micrographs of osteoblast formation on cobalt/chrome (CoCr) implant (a), and on CoCr implant with titanium coating and titanium dioxide nanotubes after 24 hours (b). Both images are 10 µm. The yellow arrows show the location of cellular extension.

Table I. Rates of calcium and phosphorus deposition by substrate

Substrate	Rate of phosphorous deposition	Rate of calcium deposition
Titanium (Ti)	0.498	0.565
Tantalum (Ta)	0.695	0.830
Ti dioxide (TiO_2) nanotubes	1.247	1.594
Ta-coated TiO_2 nanotubes	1.616	2.081

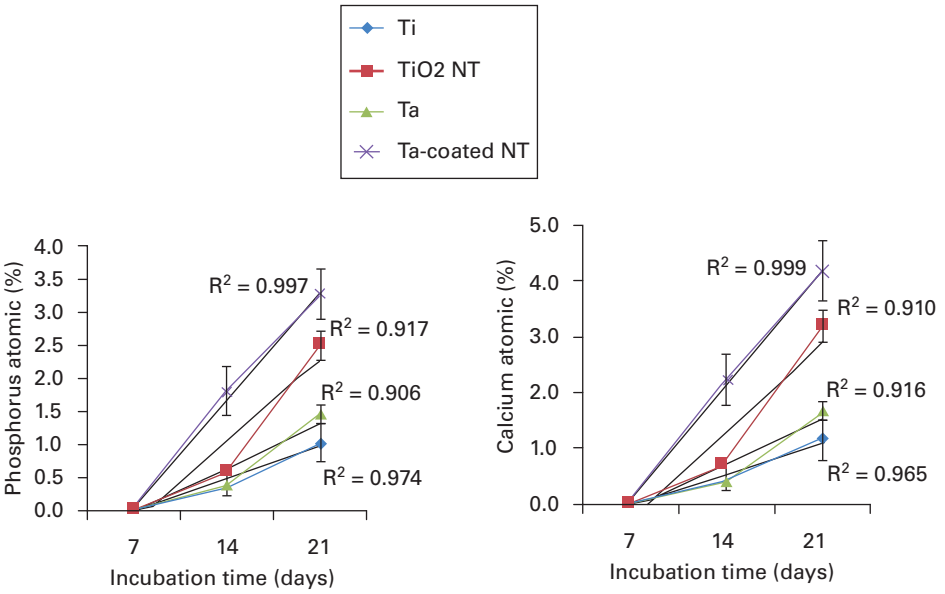

Fig. 8

Atomic percentage of phosphorus and calcium as a function of time, on titanium (Ti), tantalum (Ta), titanium dioxide (TiO_2) nanotubes (NT), and TiO_2 NT coated with Ta.

most implants today. These findings enhance our understanding of cell behaviour in response to subtle alterations in nanostructure and surface chemistry and offer further insights into the potential for compelling manipulation of biomaterial surfaces.

Antimicrobial properties

TiO_2 nanotube arrays on Ti implants have shown the additional benefit of antimicrobial capabilities. Peng et al,[21] in combination with the increased cell adhesion reported above, found in an *in vitro* evaluation that the inclusion of TiO_2 nanotubes on Ti surfaces reduced the initial adhesion

and colonisation of *Staphylococcus epidermidis* compared with polished or acid-etched Ti surfaces. Bacterial colonisation on nanotubes decreased significantly from the colonisation present on polished Ti or acid-etched Ti. The nanotubes with the larger mean diameter (80 nm) had the highest antimicrobial effect. This effect, along with the increased cell adhesion reported above, may be due to many factors, including both physical characteristics and chemical composition. It is hypothesised that the negative charge of the hydrophilic nanotube surface attaches to positively charged osteoblasts while the same surface repels the negatively charged microbes, reducing the build-up of biofilm and resisting infection. These findings show promise for clinical and commercial application, since *Staphylococcus epidermidis* is the most common pathogen associated with orthopaedic infections.[23]

Ta and silver have been shown to reduce bacterial adherence to implants.[24,25] However, the entire implant or its whole surface need not be coated with these materials to have a measureable effect. Nano-particles of silver on the surface of an implant have been shown to decrease the formation of biofilms on implants.[26-28] Apart from being bacterial resistant, nano-particles of silver are non-cytotoxic in appropriate doses and can provide long-term antimicrobial effects.[28] The fundamental idea behind this dual treatment is to enhance the osseointegration of Ti implants at the same time as improving their resistance to infection *in vivo*.

Yavari et al[26] prepared scaffolds of porous Ti with TiO_2 nanotubes by anodisation and then soaked the nanotubes in silver nitrate having low (0.02 M), medium (0.1 M), and high (0.5 M) concentrations. The antimicrobial behaviour and viability of the cells of the treated nanotube scaffolds were assessed. At up to 24 hours after treatment, the biomaterials were found to be extremely effective in preventing the formation of biofilms on the scaffolds and decreasing the number of planktonic bacteria, especially for the medium and high concentrations of silver ions. The antimicrobial effects of the biomaterials, particularly the ones with greater concentrations of antimicrobial agents, continued until two weeks however, for the groups with the highest concentrations of silver, the viability of the cells was adversely affected. The potency of the biomaterials in decreasing the number of planktonic bacteria and deterring the formation of biofilms make them promising candidates for fighting implant-associated infections.

The specific geography of a nano-textured surface can affect bacterial adhesion to the surface. Stolzoff et al[28] investigated bacterial growth on nano-textured surfaces having varied topography. Ion beam assisted deposition was used to coat Ti coupons with 0.5 μm to 1 μm of textured Ti. In order to generate varied levels of nano-texture, the energy of the argon ion beam and the density of the current were modified relative to the rate of deposition. Five samples were created with varied surface topography, although some samples had similar surface roughness. The samples were subjected to different ion energy densities, ranging from 0 mJ/cm^3 to 90.3 mJ/cm^3, to vary the surface topography. In the analysis of bacterial adhesion, samples one and two, which had negligible differences in roughness compared with samples three and five, had the greatest decrease in bacterial adhesion, while sample four, with the largest roughness was no different. The main differences in samples one and two were that their topography included evenly spaced small peaks compared with larger, more randomly positioned peaks found in samples three and five. It was concluded that the value of roughness generally did not predict the levels of bacterial colonisation. Instead, surface topography was confirmed as a key factor in the prevention of bacterial adhesion and proliferation.

In conclusion, the formation of TiO_2 nanotube arrays on Ti surfaces has been shown to increase osseointegration based on measurements of improved adhesion and propagation of osteoblasts,[19] stem cell differentiation,[15] increased elongation of cells,[17,29] higher cell density,[18] and strength of adhesion [7] when compared with non-nano-texturised Ti surfaces. The formation of TiO_2 nanotube arrays on Ti surfaces also offers improved bone mineralisation[29] and anti-microbial properties[22,26-28] compared with non-nano-texturised Ti surfaces. Additionally, TiO_2 nanotube arrays formed on Ti-coated CoCr surfaces show enhanced cell attachment.[22] When applied to orthopaedic implants, this biomimetic engineered layer may allow for earlier weight-bearing and a decreased risk of infection, thus speeding up recovery times and enhancing the health and mobility of patients. These observations suggest great promise for the development of Ti nano-texturised orthopaedic implants. In demanding applications, even the most technologically advanced macro and micro porous Ti structures can fail to integrate clinically. The potential for osseointegration of any surface is not guaranteed due to complex biological and mechanical factors. However, the surfaces of an implant that have been nano-textured with TiO_2 nanotubes show significant improvement in osseointegration.

Take home message:

- The texture of an implant surface at the nano level impacts osseointegration and anti-microbial properties.
- TiO_2 nanotube arrays are superimposed nano-texturised features on macro and micro porous tissue ingrowth surfaces.
- Macro, micro and nano texturisation is being considered for the next generation of orthopaedic joint implants.

Author contributions:

E. P. Su: Co-author, Advising surgeon, Clinical expert.
D. F. Justin: Co-author, Engineer, Principal in the company developing implants considering the technology, Principal in the company commercialising the technology.
C. R. Pratt: Co-author, Principal in the company commercialising the technology.
V. K. Sarin: Co-author, Engineer, Principal in the company commercialising the technology.
V. S. Nguyen: Advising surgeon, Clinical expert, Developer of implants considering the technology.
S. Oh: Research scientist specialising in nano-texturisation of implant surfaces who conducted much of the research and complied data.

S. Jin: Research scientist specialising in nano-texturisation of implant surfaces and other nanotechnologies, conducted much of the research and complied data, Consultant to the company commercialising the technology.

One or more of authors declare funding received from Nanovation Partners LLC that is related to this article. Nanovation Partners LLC has further developed technology licensed from the University of California San Diego, and is then licensing out the technology to the medical device industry.

The author or one or more of the authors have received or will receive benefits for personal or professional use from a commercial party related directly or indirectly to the subject of this article. In addition, benefits have been or will be directed to a research fund, foundation, educational institution, or other non-profit organisation with which one or more of the authors are associated.

This article was primary edited by J. Scott.

This paper is based on a study which was presented at the 33rd annual Winter 2016 Current Concepts in Joint Replacement meeting held in Orlando, Florida, 14th to 17th December.

References

1. **Long M, Rack HJ.** Titanium alloys in total joint replacement – a materials science perspective. *Biomaterials* 1998;19:1621–1639.
2. **Puckett SD, Taylor E, Raimondo T, Webster TJ.** The relationship between the nanostructure of titanium surfaces and bacterial attachment. *Biomaterials* 2010;31:706–713.
3. **Carr AJ, Robertsson O, Graves S, et al.** Knee replacement. *Lancet* 2012;379:1331–1340.
4. **Dalury DF.** Cementless total knee arthroplasty. *Bone Joint J* 2016; 98-B:867–873.
5. **Drees P, Eckardt A, Gay RE, Gay S, Huber LC.** Mechanisms of disease: molecular insights into aseptic loosening of orthopedic implants. *Nat Clin Pract Rheumatol* 2007;3:165–171.
6. **Bordini B, Stea S, De Clerico M, et al.** Factors affecting aseptic loosening of 4750 total hip arthroplasties: multivariate survival analysis. *BMC Musculoskelet Disord* 2007;8:69.
7. **Bjursten LM, Rasmusson L, Oh S, et al.** Titanium dioxide nanotubes enhance bone bonding in vivo. *J Biomed Mater Res A* 2010;92:1218–1224.
8. **No authors listed.** National Nanotechnology Initiative, What's So Special about the Nanoscale? https://www.nano.gov/nanotech-101/special (date last accessed 21 August 2017).
9. **Jin S, Oh S.** Compositions comprising nanostructures for cell, tissue and artificial organ growth, and methods for making and using same. United States Patent 8414908. 9 April 2013. https://www.google.com/patents/US8414908 (date last accessed 30 August 2017).
10. **Zwilling V, Darque-Ceretti E, Boutry-Forveille A, et al.** Structure and physicochemistry of anodic oxide films on titanium and TA6V alloy. *Surf Interface Anal* 1999;27:629–637.
11. **Gong D, Grimes CA, Varghese OK, et al.** Titanium oxide nanotube arrays prepared by anodic oxidation. *J Mater Res* 2001;16:3331–3334.
12. **Varghese OK, Gong D, Paulose M, Grimes CA, Dickey EC.** Crystallization and high-temperature structural stability of titanium oxide nanotube arrays. *J Mater Res* 2003;18:157–165.
13. **Mor GK, Varghese OK, Paulose M, Mukherjee N, Grimes CA.** Fabrication of tapered, conical-shaped titania nanotubes. *J Mater Res* 2003;18:2588–2593.
14. **Cai Q, Paulose M, Varghese OK, Grimes CA.** The effect of electrolyte composition on the fabrication of self-organized titanium oxide nanotube arrays by anodic oxidation. *J Mater Res* 2005;20:230–236.
15. **Oh S, Brammer KS, Li YSJ, et al.** Stem cell fate dictated solely by altered nanotube dimension. *Proc Natl Acad Sci USA* 2009;106:2130–2135.
16. **Descamps S, Awitor KO, Raspal V, et al.** Mechanical properties of nanotextured titanium orthopedic screws for clinical applications. *J Med Device* 2013;7:210051–210055.
17. **Frandsen CJ.** An extensive analysis of modified nanotube surfaces for next-generation orthopedic implants. http://escholarship.org/uc/item/4v60v29j?query=frandsen (date last accessed 21 August 2017).
18. **Brammer KS.** Controlled nanostructures for enhanced biological responses and release of incorporated biomolecules. http://escholarship.org/uc/item/9612567k#page-1 (date last accessed 21 August 2017).
19. **Oh S, Daraio C, Chen LH, et al.** Significantly accelerated osteoblast cell growth on aligned TiO_2 nanotubes. *J Biomed Mater Res A* 2006;78:97–103.
20. **Gongadze E, Kabaso D, Bauer S, et al.** Adhesion of osteoblasts to a nanorough titanium implant surface. *Int J Nanomedicine* 2011;11:1801–1816.
21. **Peng Z, Ni J, Zheng K, et al.** Dual effects and mechanism of TiO2 nanotube arrays in reducing bacterial colonization and enhancing C3H10T1/2 cell adhesion. *Int J Nanomedicine* 2013;8:3093–3105.
22. **Frandsen CJ, Brammer KS, Noh K, Johnston GW, Jin S.** Tantalum coating on TiO2 nanotubes induces superior rate of matrix mineralization and osteofunctionality in human osteoblasts. *Mater Sci Eng C Mater Biol Appl* 2014;37:332–341.
23. **Valour F, Trouillet-Assant S, Rasigade J- P. .***Staphylococcus epidermidis* in orthopedic device infections: the role of bacterial internalization in human osteoblasts and biofilm formation. *PLoS One* 2013;8:67240.
24. **Schildauer TA, Robie B, Muhr G, Köller M.** Bacterial adherence to tantalum versus commonly used orthopaedic implant materials. *J Orthop Trauma* 2006;20:476–484.
25. **Li H, Cui Q, Feng B, et al.** Antibacterial activity of TiO2 nanotubes: influence of crystal phase, morphology and Ag deposition. *Appl Surf Sci* 2013;284:179–183.
26. **Amin Yavari S, Loozen L, Paganelli FL, et al.** Antibacterial behavior of additively manufactured porous titanium with nanotubular surfaces releasing silver ions. *ACS Appl Mater Interfaces* 2016;8:17080–17089.
27. **Shivaram A, Bose S, Bandyopadhyay A.** Mechanical degradation of TiO2 nanotubes with and without nanoparticulate silver coating. *J Mech Behav Biomed Mater* 2016;59:508–518.
28. **Stolzoff M, Burns JE, Aslani A, et al.** Decreased bacterial growth on titanium nanoscale topographies created by ion beam assisted evaporation. *Intl J Nanomedicine* 2017;12:1161–1169.
29. **Ni J, Frandsen CJ, Noh K, et al.** Fabrication of thin film TiO2 nanotube arrays on Co-28Cr-6Mo alloy by anodization. *Mater Sci Eng C Mater Biol Appl* 2013;33:1460–1466.

Stem cell fate dictated solely by altered nanotube dimension

Seunghan Oh[a], Karla S. Brammer[a], Y. S. Julie Li[b], Dayu Teng[b], Adam J. Engler[b,c], Shu Chien[b,c,1], and Sungho Jin[a,c,1]

Departments of [a]Materials Science and Engineering and [b]Bioengineering, and [c]Institute of Engineering in Medicine, University California at San Diego, La Jolla, CA 92093

Contributed by Shu Chien, December 24, 2008 (sent for review December 4, 2008)

Two important goals in stem cell research are to control the cell proliferation without differentiation and to direct the differentiation into a specific cell lineage when desired. Here, we demonstrate such paths by controlling only the nanotopography of culture substrates. Altering the dimensions of nanotubular-shaped titanium oxide surface structures independently allowed either augmented human mesenchymal stem cell (hMSC) adhesion or a specific differentiation of hMSCs into osteoblasts by using only the geometric cues, absent of osteogenic inducing media. hMSC behavior in response to defined nanotube sizes revealed a very dramatic change in hMSC behavior in a relatively narrow range of nanotube dimensions. Small (≈30-nm diameter) nanotubes promoted adhesion without noticeable differentiation, whereas larger (≈70- to 100-nm diameter) nanotubes elicited a dramatic stem cell elongation (≈10-fold increased), which induced cytoskeletal stress and selective differentiation into osteoblast-like cells, offering a promising nanotechnology-based route for unique orthopedics-related hMSC treatments.

differentiation | mesenchymal | nanotopography | osteogenesis | proliferation

Nanostructures are of particular interest because they have the advantageous feature of a high surface-to-volume ratio, and they elicit a higher degree of biological plasticity compared with conventional micro- or macrostructures. In the field of biomaterial development and in vivo implant technology, the nanoscale structure and morphologenic factor of the surface have played a critical role in accelerating the rate of cell proliferation and enhancing tissue acceptance with a reduced immune response (1, 2). In terms of in vitro cell biology, there has also been much attention placed on cellular responses to their structural surroundings (3). In fact, it has been observed that macro-, micro- and nano-sized topographical factors stimulate behavioral changes in both cells and tissues. Recent studies related to the effect of nanotopography on cellular behavior indicated that osteoblast adhesion and functionality was enhanced by 30% when cultured on a nanograined Al_2O_3 and TiO_2 substrate (4–6) compared with those cultured on a micrograined surface, and nanostructures such as TiO_2 nanotubes with <100-nm spacing showed superior characteristics in bone mineral synthesis (5). However, most of the previous studies on nanostructures and cell responses have mainly used oriented, patterned, or semiordered polymer arrays (7–9) and alumina/polymer hybrid patterned arrays (10).

The material and mechanical characteristics of titanium (Ti) metal, which has a thin native oxide layer of TiO_2, make it an ideal orthopedic material that bonds directly to the adjacent bone surface (11, 12). Fabrication of the nanostructured titanium dioxide (TiO_2) nanotube arrays has been a primary subject of investigation lately because of the wide range of TiO_2 applications in the fields of solar cells (13–16), photocatalysis (17–19), photoelectrolysis (20), sensors (21, 22), and biomaterials (23–25). The presence of a vertically aligned TiO_2 nanotube surface on Ti foils had a critical effect that improved the proliferation and mineralization of osteoblasts (24) and enhanced the mobility, vasodilation, and monolayer formation of endothelial cells (25) because of the unique nanotopographical features and high biocompatibility of the TiO_2 nanotube surface.

Several recent studies have investigated the influence of nanostructures on mesenchymal stem cell (MSC) proliferation and differentiation into specific cell lineages. It is well known that MSCs are multipotent stem cells that can differentiate into stromal lineages such as adipocyte, chondrocyte, fibroblast, myocyte, and osteoblast cell types by generating the appropriate intermediate progenitors for each. By examining the cellular behavior of MSCs cultured in vitro on nanostructures, it can provide some indication and understanding of the effects that the nanostructures may have on the stem cell's response, and possibly how to direct the formation of bone in vivo. Most previous studies have used the combination of osteogenic inducing media having additional chemical factors and nanostructured culture substrates to accelerate osteogenesis and bone formation of MSCs in vitro, but it is difficult to truly distinguish whether the effect of the nanostructured surface topography itself can achieve MSC differentiation without adding chemical factors. Here, we demonstrate that TiO_2 nanotube size can regulate human mesenchymal stem cell (hMSC) differentiation toward an osteoblast lineage in the absence of osteogenic inducing factors and we describe a mechanism for controlling MSC fate based on a narrow range of nanotube dimensions.

Results

We prepared nominally 30-, 50-, 70-, and 100-nm TiO_2 nanotubes on Ti substrates by anodization (25), as depicted in Fig. 1, to determine how the size of the nanotubes would play a role in the cellular response and differentiation of hMSCs [detailed experimental descriptions can be found in *Materials and Methods* and in supporting information (SI) *Materials and Methods*]. The self-assembled TiO_2 nanotube arrays on Ti substrates have a robust and discrete shape, confirmed by SEM images, which show highly ordered nanotubes with 4 different pore sizes between 30 and 100 nm that were created by controlling anodizing potentials (5, 10, 15, and 20 V). Flat Ti substrates (having a native TiO_2 oxidation layer on the surface with analogous chemical composition of the nanostructured TiO_2 substrates) were used as comparison substrata. SEM images of hMSCs cultured on experimental substrata showed that, after 2 and 24 h of incubation, the shape of the hMSCs sitting on top of flat Ti and on various sizes of TiO_2 nanotubes were extremely different (Fig. 2). hMSCs on flat Ti appeared to be more round and stationary; they lacked the noticeable filopodia extensions and cellular propagation fronts like those cultures on TiO_2 nano-

Author contributions: S.O., A.J.E., S.C., and S.J. designed research; S.O. and K.S.B. performed research; A.J.E. contributed new reagents/analytic tools; Y.S.J.L., D.T., S.C., and S.J. analyzed data; and S.O., K.S.B., Y.S.J.L., D.T., S.C., and S.J. wrote the paper.

The authors declare no conflict of interest.

[1]To whom correspondence may be addressed. E-mail: shuchien@ucsd.edu or jin@ucsd.edu.

This article contains supporting information online at www.pnas.org/cgi/content/full/0813200106/DCSupplemental.

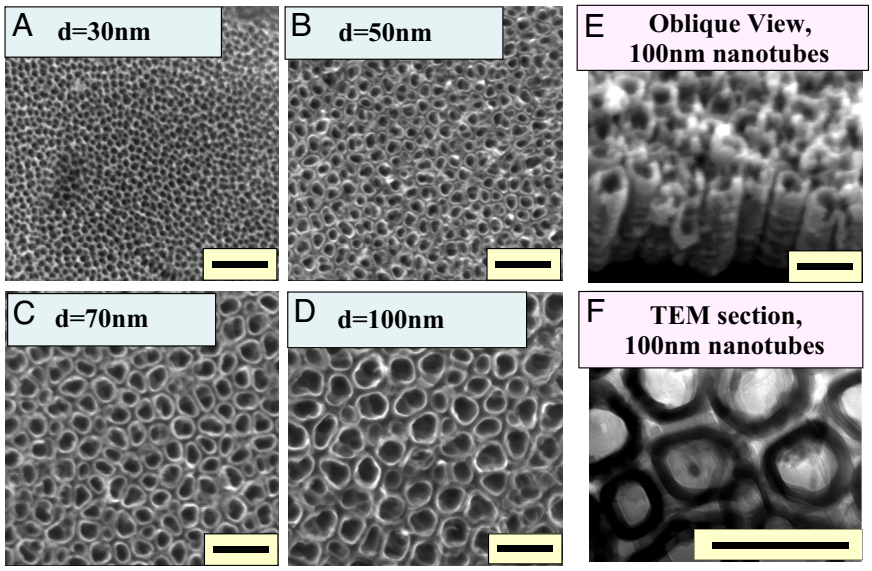

Fig. 1. TiO_2 nanotube. (*A–D*) SEM micrographs (top view) of self-aligned TiO_2 nanotubes with significantly different diameters. The self-assembly layers were generated by anodizing Ti sheets. The images show highly ordered, vertically aligned nanotubes with 4 different nanotube pore diameters, 30, 50, 70, and 100 nm, created by controlling anodizing potentials ranging from 5 to 20 V. (*E*) SEM micrographs (oblique view) of the 100-nm diameter TiO_2 nanotube. (*F*) Cross-sectional transmission electron microscopy (TEM) of the 100-nm diameter TiO_2 nanotubes. (Scale bar, 200 nm.)

tubes. However, on nanotube surfaces especially for the cases of larger-diameter nanotubes, a large number of prominent filopodia and unidirectional lamellipodia extensions were apparent on the nanotube structures even after just 2 h of culture (Fig. 2 *Upper*). This trend becomes much more apparent if the hMSC culture time is extended to 24 h (Fig. 2 *Lower*), and significantly more pronounced when the nanotube diameter is increased (lamellipodia are shown by the yellow arrows). As indicated by the red arrows, hMSCs exhibit cellular morphologies with extraordinary elongation of as much as 200 μm in length on 100-nm TiO_2 nanotube surfaces. This is $\approx$10-fold increase in the hMSCs cellular elongation length compared with the identical culture conditions for the 30-nm nanotubes.

Higher magnification SEM images of TiO_2 nanotube substrata (Fig. 3) after 2 h of culture reveal the adhesion of many round protein aggregates, $\approx$30 nm in diameter, deposited from serum in the culture media. These protein aggregates are most likely settling on the surface, acting as a preexisting, accessible protein coating, which would have implications on how the cells initially perceive the surface and the way they attach. Protein aggregates are rather quickly deposited after only 2 h of incubation on the wall top of the nanotubes. Less protein aggregate deposition, with a sparse distribution, is observed on flat Ti samples, whereas aggregate coating of the Ti nanotubes directly scales with nanotube diameter.

The cell adhesion and elongation aspects were further studied to elucidate the nanotube size dependence of hMSC behavior.

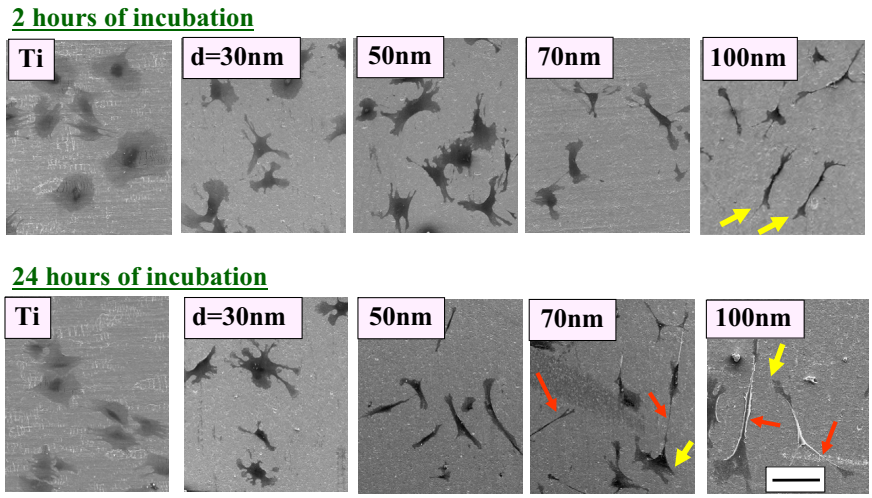

Fig. 2. SEM micrographs of human mesenchymal stem cells (hMSCs) on flat Ti and 30-, 50, 70-, and 100-nm diameter TiO_2 nanotube surfaces after 2 h of culture. (Scale bar, 100 μm.) Cells are flat, spread out, and round-shaped on the flat Ti substrate, they are somewhat flat and rounded on 30-nm nanotubes, and they become progressively elongated as the nanotube diameter is increased to 50-nm diameter and beyond. Extraordinary cell elongation is induced on nanotubes with diameters of 70 and 100 nm (see red arrows), especially after the 24 h culture. More mobile morphologies are indicated by the presence of somewhat elongated leading edges of lamellipodia (yellow arrows) seen on 70 and 100 nm nanotubular surfaces. The cell shapes suggest that cells are more elongated on the bigger TiO_2 nanotubes.

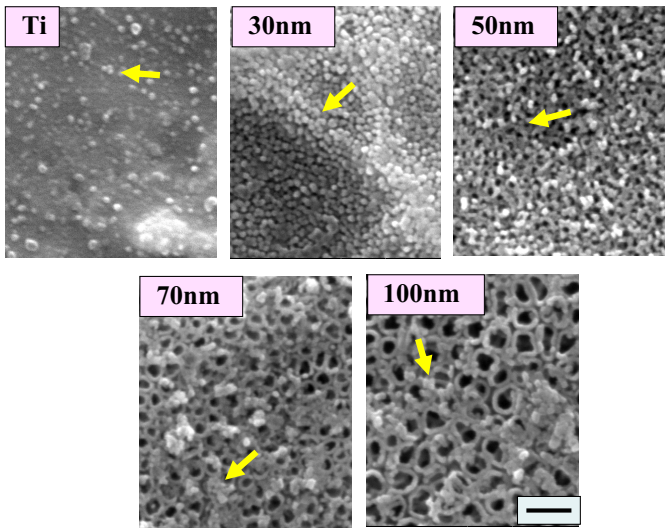

Fig. 3. SEM micrographs showing extracellular matrix aggregates on the surfaces of flat Ti and 30-, 50-, 70-, and 100-nm diameter TiO_2 nanotubes after 2 h of hMSC culture. (Scale bar, 200 nm.) Note that the presence of protein aggregates is infrequent on Ti, abundant on 300-nm nanotubes, and much less on the larger-diameter 70- and 100-nm nanotubes.

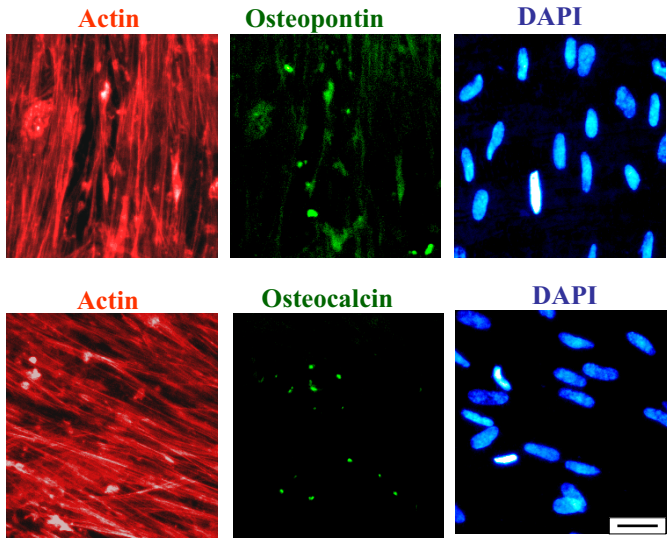

Fig. 4. Immunofluorescent images of OPN (*Upper Center*) and OCN (*Lower Center*), as well as actin (*Left*) and DAPI (*Right*), on 100-nm diameter TiO_2 nanotubes after 3 weeks of culture. (Scale bar, 50 μm.)

As shown in Fig. S1*a*, it became apparent that the number of adhered hMSCs on the experimental substrata decreased almost inversely proportional to the pore size of the TiO_2 nanotubes at the critical early stage of hMSC interaction with substrata (within the initial 24 h of incubation time). After prolonged incubation, cell growth for all other substrates caught up and these differences eventually were not as apparent because of the confluency of the cells, as might be anticipated at 7 days of culture time.

To understand the relationship between the nanodimensional cues and hMSC cell behavior, we also carried out a quantitative analysis of cellular morphological elongation. As shown in Fig. S1*b*, the elongation ratio of hMSCs increased with increasing size of TiO_2 nanotubes. The largest TiO_2 nanotubes showed an average elongation ratio of length/width as large as $\approx$10, whereas the small-diameter nanotubes of 30 nm (as well as the flat Ti) exhibited a basically isotropic configuration with an overall average elongation ratio of more or less $\approx$1. These cell elongation results were also confirmed with live cell imaging by using fluorescein diacetate (FDA) staining, which is shown in Fig. S2. The extraordinary stretching of hMSCs for the larger-diameter nanotubes of 70 and 100 nm is evident from the figure and demonstrate that cell elongation and adhesion appear to be inversely related to one another on Ti nanotubes.

The elongation/stretching of the hMSCs on larger-diameter nanotubes resulted in a preferential differentiation into osteogenic lineage, which was confirmed by immunofluorescent staining of 2 common protein osteogenetic markers: osteopontin (OPN) and osteocalcin (OCN). This analysis for the detection of osteogenic protein expression of hMSCs was conducted on cells cultured for 21 days. The immunofluorescent results, which are given in Fig. 4 for 100-nm TiO_2 nanotubes, showed that hMSCs had recognizable OCN- and OPN-positive staining with staining shapes associated with osetoblast cells, whereas hMSCs on the much smaller-diameter nanotubes and flat Ti substrata did not elicit any positive staining. Fig. 4 *Upper* represents osteopontin (OPN) staining (together with actin and dapi staining for the same image area to also illustrate the cytoplasmic actin skeleton and cell nuclei), whereas Fig. 4 *Lower* shows the osteocalcin (OCN) staining (again with actin and dapi staining of the same image area).

To further support the immunofluorescent staining results described above, osteoblast gene expression (OCN, osteocalcin; OPN, osteopontin; and ALP, alkaline phosphatase) was also studied by quantitative real-time PCR analysis after 14 days of incubation, with the analysis data shown in Fig. 5. hMSCs on 70- and 100-nm TiO_2 nanotubes demonstrated various levels of osteogenic up-regulation and showed a significantly higher level of expression than those on other substrata ($P < 0.01$). The 100-nm nanotubes displayed the highest up-regulation of all selected osteoblastic genes among the experimental groups at just 14 days of incubation and were closest to chemically induced osteoblast gene expression (positive control). Together, immunofluorescence and real-time PCR results seemed to confirm that 100-nm nanotubes have the potential as a guided differentiation tool for directing hMSCs into osteoblast-like cells in the absence of osteogenesis-inducing media. In contrast, the 30-nm nanotube sample exhibited a significantly lower degree of almost negligible osteoblast gene expression (considering the magnitude of error bars), as indicated in Fig. 5.

Discussion

Serum is widely used in the culturing of eukaryotic cells and it is known to contain many extracellular matrix globular proteins

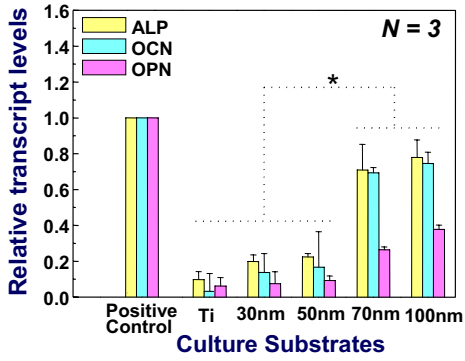

Fig. 5. Quantitative PCR analysis for ALP, OCN, and OPN. Plastic cell culture plate with osteogenic inducing media was used as a positive control for osteogenic differentiation. *, Significant differences between Ti, 30- and 50-nm nanotubes vs. 70- and 100-nm nanotubes for ALP, OCN, and OPN gene expressions ($P < 0.01$).

and glycoproteins as major components. Immunofluorescent staining for 2 serum proteins, BSA and fibronectin, on the sample surfaces after 2 h of incubation in media revealed positive results for both proteins. Fibronectin was detected on the surfaces (Fig. S3) as well as albumin. Fibronectin, which is known to play a major role in cell adhesion, is a high-molecular-weight glycoprotein, which when in solution coils up into a nanometer-sized aggregate. The size of albumin is well known to also be several nanometers, which may have been agglomerated/conformed in the ≈30- to 60-nm size on top of the sample surfaces during the ≈2 h of incubation time. Although further studies are needed to identify the detailed nature of the protein attached to the nanotube surface, we clearly demonstrate that there is a significant dependence of protein attachment on nanotube absent of any chemical stimulus. The serum in our experimentation is identical to that used by Dalby *et al.* (7).

It is reasonable that the control surface, i.e., flat Ti (with a TiO_2 native oxide layer), has a lower population of these protein aggregates, because it is less hydrophilic than the higher-surface-area TiO_2 nanotube surfaces, in general, based on water droplet contact angle measurements. It would be interesting to perform additional studies on the effect of hydrophilicity of TiO_2 nanotubes on cell and protein adhesion and growth. From the nanoscale perspective, the nanotubes are generally of uniform height and diameter, although there are slight variations. On microscopic scales, however, there could be some local nonuniform heights due to the surface roughness of the starting material and various process steps, such as substrate anodization, addition of serum-containing media, and associated protein (i.e., fibronectin) adsorption. Atomic force microscopy analyses indicate that the variations in the processed sample surface height >20-μm scan are $<$ ≈200 nm, which may be viewed as being insignificant from the context of what a cell sees. Because sharp edges are known to create spots of high surface energy to facilitate focal adhesion, further studies are needed to clarify how much, if any, such nonuniformity in nanostructure affects the hMSC adhesion to TiO_2 nanotube substrates.

Among the various sizes of TiO_2 nanotubes, the smaller-dimension nanotubes of 30-nm diameter, and to some extent for the 50-nm TiO_2 nanotubes, showed a much higher population of protein aggregates on the top surface when compared with nanotubes with 70-nm or 100-nm diameter. The 30-nm diameter nanotubes, in particular, elicit complete substrate surface coverage with the protein aggregates. The reason for the much reduced protein aggregate adsorption observed on the top of larger-diameter nanotubes of 70- and 100-nm diameter is most likely because ≈30-nm size protein aggregates are just too small to anchor on 70- or 100-nm diameter nanopores with much larger open pore spaces, because the protein aggregates initially attach only to the available surfaces that are the top portion of the nanotube walls. We believe that we have found a threshold point of nanotube size (≤50 nm) where the adhesion of proteins (≈30-nm-size regime) initially determines the degree of cell adhesion, a critical observation in this study. The phenomenon of initial protein adsorption is very important in understanding why hMSCs were more elongated on the 100-nm nanotube surface than hMSCs on the smaller-sized nanotube surfaces. Extracellular matrix (ECM) proteins are required for a cell to adhere to the surface and to be able to spread out. Within an initial incubation time (say, <6 h), the proteins available in the culture media from the serum adsorb to the surface and act as the preliminary ECM, which can help cell adhesion considerably at the earliest stages of culture before cells begin secreting their own ECM. hMSCs cultured on <50-nm TiO_2 nanotubes can more easily attach to the surface because of the high population of ECM proteins deposited across the entire surface as indicated in Fig. 3. However, hMSCs cultured on 100-nm TiO_2 nanotubes probably would have to struggle to search for areas where more protein aggregates have been deposited to establish initial contact because there is much more interprotein aggregate spacing due to the large pore sizes in the nanostructure. Eventually, the hMSCs have to extend their filopodia extensions excessively and move to find proteins, thus becoming more mobile and forming more extraordinarily elongated shapes.

For further understanding of the hMSC elongation behavior and related effect on stem cell differentiation, 2 possible routes of systematic investigations could be used in the future to force the hMSCs to elongate into specific commanded dimension. These include (*i*) dictating the substrate dimensional cues with selected line pattern width for control of hMSC cell width and elongation (for example, by using hMSC adherent line region separated by hMSC-repelling regions such as coated with polyacrylamide gel), and (*ii*) dictating the distance that the hMSCs need to travel and stretch by using the intentionally spaced extracellular islands [for example, by providing a periodically placed ECM island array pattern (e.g., in a triangular array configuration by nanoimprint stamping transfer)] that would dictate how much the hMSCs have to stretch out to reach the next available ECM island(s). Such experiments can further elucidate the effect of artificially controllable geometrical cues on stem cell enrichment or differentiation, and may provide valuable bioengineering methodologies for stem cell control and beneficial therapeutic applications.

It is notable that the hMSCs adhered to the smallest dimensioned 30-nm nanotubes more efficiently in the first 2 h probably because of the high protein population initially on the surface (Fig. S1*a*). Also noticeable in the figure is that the highest quantity of adhered and growing hMSC cells was maintained on the 30-nm nanotube substrates after the first 24 h of incubation. However, in comparison, as indicated in the SEM micrographs and FDA images, the larger-diameter nanotubes (70- and 100-nm diameter) that induced a dramatic cell elongation increased osteogenic expressions (Figs. 4 and 5) with a lower amount of adhered cells.

We have described in previous studies (24) that the long-range structure of TiO_2 nanotubes is neither patterned nor highly ordered, but they do have a robust and discrete nanotube shape. Dalby *et al.* (7) reported that MSC cultured on highly ordered poly(methylmethacrylate) (PMMA) nanopatterns showed negligible osteogenic differentiation, but randomized PMMA nanotopography demonstrated MSC osteoblastic morphologies after 21 days of incubation with cell growth media. We have similarly demonstrated, with our nonordered TiO_2 nanotube arrays, results that are in agreement with their findings where hMSC osteogenic differentiation is observed without osteogenic inducing media. However, we demonstrate in this report a clear mechanism for MSC fate based on the TiO_2 nanotube geometry providing an explanation for control of MSCs by specific nanotube dimensions.

This observed attainment of differentiation in the absence of additional biochemical inducing agents is critical to the success of our nanotopography-induced differentiation shown in the following results. Many biochemists and molecular biologists induce differentiation by chemical factors in vitro, but there is no well-understood way of controlling such factors and precise concentrations in vivo. In fact, the side effects of many chemicals such as dexamethasone or β-glycerophosphate, typical osteogenic inducing reagents, are not known because the body does not encounter these types of chemicals naturally. In contrast, our approach relies on controlling stem cell fate by using only the nanotopography, which is much more dependable, and we can expect a similar and more reproducible in vivo response because we do not have the in vivo variability and side effects associated with chemical additions.

In terms of the correlation between initial cell density and differentiation of mesenchymal stem cells, Pittenger *et al.* (27)

and McBeath *et al.* (28) reported that initial cell-plating density made critical effects on the differentiation of mesenchymal stem cells, and a lower cell density showed better osteoblastic differentiation compared with a higher cell density in the presence of osteogenic inducing media. From our results we have shown that 100-nm nanotubes elicited a lower initial cell number (Fig. S1*a*), but a higher osteogenic gene expression than other sizes of nanotubes (Fig. 5). Although the final cell density eventually saturates after a longer incubation and becomes essentially the same for different diameter nanotubes, it is likely that the initial cell density has a lasting impact on the eventual stem cell fate. From this point of view, we too show a correlation between cell density and differentiation and can draw some similarity between Pittenger *et al.* and McBeath *et al.*'s observations (27, 28) and our findings.

Furthermore, our experimental results indicated that the hMSCs were extraordinarily more stretched and probably stressed on the 100-nm nanotubes, ≈10 times longer in average cell length than those on the 30-nm nanotubes as shown in the SEM micrographs of Fig. 2. It is most probable that this elongated morphology causes cellular cytoskeletal tension and stress on the hMSCs cultured on 70- to 100-nm diameter regime nanotubes compared with a normal cell culture condition on a flat surface substrate. It is well known that various kinds of physical stresses from the substrate morphology and topography can accelerate stem cell differentiation into a specific cell lineage (29–35); our data show a similar scenario.

In addition, the SEM and FDA images of hMSCs on all sizes of TiO_2 nanotubes showed the formation of more filopodia, lamellipodia, and cellular extensions compared with those on flat Ti. Our results are also in general agreement with other studies relating cellular extensions and differentiation (7, 8).

The trends of hMSC adhesion, elongation, and differentiation behavior reported here as a function of nanotube dimension seem to reveal a specific mechanism that determines the stem cell fate solely on the geometric cues of the surface. The mechanism follows that, on small-diameter nanotubes, increased cell adhesion and growth with minimal differentiation seem to be prevalent, because this is in part due to the protein aggregate adhesion configurations induced by the small nanotubes. On larger-diameter nanotubes, hMSC cells are forced to elongate and stretch to search for protein aggregates, and as a result, are forced/guided to differentiate specifically into osteoblast cells. This claim is based on the well-established research that shows when stem cells are stressed due to the high elastic modulus, for example, stiff substrates; differentiation into osteoblast cells is enhanced (7, 8, 32). From the results of our research, we have developed a concept of stem cell fate based on nanotube dimension and it is schematically illustrated in Fig. 6, with the protein aggregate dimensions and hMSC elongation trends also incorporated. This suggested mechanism is, in a sense, in agreement with the general notion that when cells are busy adhering and growing, their functionality is expected to be reduced, and when the stem cells are stressed, they tend to differentiate into a specific lineage to accommodate the stress.

Although the hMSC growth and differentiation behavior appear to be somewhat saturating at ≈100-nm diameter, it would nevertheless be interesting to investigate their behavior on larger-diameter TiO_2 nanotubes so as to find an ultimate saturation limit of stem cell differentiation. However, it is noted that such larger-diameter TiO_2 nanotubes beyond the ≈100 nm regime are currently difficult to fabricate by the same self-assembly anodization processing techniques used here, and hence new process approaches are needed to enable such a study.

This research elucidates the effects of the nanotopography of TiO_2 nanotubes on mesenchymal cell adhesion, morphology, and osteogenic differentiation, all in the absence of osteogenic media. We have made a striking discovery that the cell adhesion and growth (without differentiation) vs. guided differentiation is strongly correlated with the size of nanotubes in a relatively small window of nanotube diameter ranges. We also demonstrate that a guided osteogenic differentiation of hMSCs can be controllably manipulated by selective sizing of the nanotube dimensions. Because the TiO_2 nanotubes are excellent osseointegration biomaterials as evidenced by in vitro data (24), and our preliminary in vivo animal data indicating a strong new bone integration on the nanotube surface with reduced soft tissue trapping (data not shown), the nanotube surface can perform dual therapeutic functions of specifically guided differentiation and strong osseointegration for new bone formation. We forecast that these results can be a milestone for the further study of stem cell control and implant development, in terms of its application as a therapeutic platform as well.

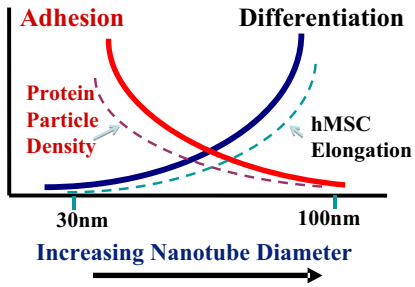

Fig. 6. Schematic illustration of the overall trends of nano cue effects on hMSC fate and morphology after a 24-h culture. The change in hMSC cell adhesion and growth without differentiation (solid red line) has the same trend as protein particle density (broken red line), whereas that of differentiation (solid blue line) has the same trend as hMSC elongation (broken blue line).

Materials and Methods

TiO_2 Nanotube Fabrication. The protocol for preparation of TiO_2 nanotubes by anodization process for cell culture is similar to what we used (5, 24, 25) and is described as follows. The nanotubes were formed on a Ti sheet (Alfa-Aesar; 0.25 mm thick, 99.5%) by using a mixture of 0.5 wt % hydrofluoric acid (EM Science; 48%) and acetic acid (Fisher; 98%, volumetric ratio = 7:1) at 5, 10, 15, and 20 V for 30 min to obtain different diameter nanotubes. A platinum electrode (Alfa-Aesar; 99.9%) served as the cathode. The specimen was rinsed by deionized water, dried at 80 °C, and heat treated at 500 °C for 2 h to transform the as-anodized amorphous TiO_2 nanotubes into crystalline phase. The specimens (1.27 × 1.27 cm^2 area) used for all experiments were sterilized by autoclaving before use. An identically sized flat Ti sample was used as a control after being chemically cleaned by acetone and isopropyl alcohol, dried, and autoclaved.

Cell Culture. Human mesenchymal stem cells (hMSCs) were obtained from Lonza Corporation. The cell growth media were composed of α-MEM (Invitrogen), 10% Fetal Calf Serum (FCS) (Invitrogen), 100 units/mL penicillin, and 100 μg/mL streptomycin (Invitrogen). For preparing positive control in this research, osteogenic inducing media were also prepared by adding 10 nM dexamethasone (Sigma), 150 μg/mL L-ascorbic acid (Sigma), and 10 mM β-glycerophosphate (Calbiochem) to cell growth media. The cells were cultured in a 5% CO_2 incubator at 37 °C. All experiments of hMSCs were conducted with cultures at passage 4.

Scanning Electron Microscopy (SEM) for Substrate and Cell Morphological Examination. Initially cells were plated on the substrates at a density of 1×10^4 cells per mL. After 2 h of culture, the cells on the substrates were washed with 1× PBS and fixed with 2.5% glutaraldehyde in 0.1× PBS for 1 h. After fixation, they were washed 3 times with 1× PBS for 10 min each wash. Then the cells were dehydrated in a graded series of ethanol (50, 70, 90, and 100%) for 30 min each and left in 100% ethanol until they were dried by supercritical point CO_2. Next, the dried samples were sputter-coated with very thin gold for SEM examination. The morphology of the TiO_2 nanotubes, as well as that of the adhered cells, was observed by using SEM (XL30, FEI Corporation).

Immunofluorescence of Actin and Osteopontin/Osteocalcin. After 3 weeks of culture, the cells on the Ti and TiO_2 nanotube substrates were fixed in 4% paraformaldehyde in 1× PBS for 15 min at room temperature. Once fixed, the cells were washed twice with 1× wash buffer (1× PBS containing 0.05% Tween-20). To permeablilize the cells 0.1% Triton X-100 in 1× PBS solution was added for 10 min. The cells were washed twice with wash buffer. Then the samples were incubated for 1 h at room temperature in 1% BSA/1× PBS followed by the addition of antiosteopontin (OPN) antibody (1:100, AKm2A1, Santa Cruz Biotechnology)/antiosteocalcin (OCN) antibody (1:100, OC4–30, QED Bioscience), and incubated for overnight at 4 °C. After incubation, cells were washed 3 times for 5 min each wash with 1× wash buffer. Goat anti-mouse IgG-FITC (1:100, Santa Cruz Biotechnology) and TRITC-conjugated phalloidin (1:40, Invitrogen) in 1× PBS was added for double staining and the cells were incubated again for 1 h at room temperature. The cells were washed 3 times with 1× wash buffer for 5 min each wash. Then, the samples were stained by DAPI (1:1000, Chemicon) for nucleus staining. The samples were then inverted onto coverslips mounted, visualized, and photographed by an epifluorescence microscope (DM IRB, Leica Microsystems).

Real-Time PCR. After 2 weeks of culture, total RNA of the cells on the Ti and TiO_2 nanotube substrates were extracted with TRIzol (Sigma), and reverse-transcribed into cDNA by qScript cDNA Synthesis Kit (Quanta BioSciences). Real-time PCR was performed by Taqman Gene Expression Assays (Applied Biosystems), and the information of Taqman PCR primer is as follows: GAPDH (Hs99999905_m1; Amplicon length, 122), ALP (Hs01029141_g1; Amplicon length, 71), OCN (Hs00609452_g1; Amplicon length, 74) and OPN (Hs00960942_m1; Amplicon length, 63). Real-time PCR was carried out by using Taqman Fast Universal PCR Master Mix and 7900 HT Fast Real-Time PCR System (Applied Biosystems). cDNA samples (1 μL for total volume of 20 μL) were analyzed for gene of interest and for house-keeping gene GAPDH. The comparison test of cycle-threshold point was used to quantify the gene expression level of each sample. In this study, all levels of expression were normalized by the level of expression of positive control (hMSCs cultured with osteogenic inducing media).

Statistical Analysis. In terms of cell count, cell elongation, and real-time PCR assay, all data were expressed as mean ± standard error, and analyzed statistically by the paired Student's *t* test method. Significant difference was determined at P values at least <0.01.

ACKNOWLEDGMENTS. We thank S. Chirasatitsin for assistance in atomic force microscopy analysis. The hMSC experiments were carried out at Human Stem Cell Core Facility at University of California at San Diego. This work was supported in part by California Institute for Regenerative Medicine (CIRM) Postdoctoral Fellowship (S.O.) and Seed Grant RS1-00172–1-(to S.C.), National Institutes of Health Grant HL-080518 (to S.C.), and the Iwama Endowed Fund at University of California at San Diego (S.J.).

1. Jung DR, *et al.* (2001) Topographical and physicochemical modification of material surface to enable patterning of living cells. *Crit Rev Biotechnol* 21(2):111–154.
2. Mahdavi A, *et al.* (2008) A biodegradable and biocompatible gecko-inspired tissue adhesive. *Proc Natl Acad Sci USA* 105:2307–2312.
3. Curtis AS, Varde M (1964) Control of cell behavior: Topological factors. *J Natl Cancer Inst* 33:15–26.
4. Webster TJ, Ergun C, Doremus RH, Siegel RW, Bizios R (2000) Enhanced functions of osteoblasts on nanophase ceramics. *Biomaterials* 21(17):1803–1810.
5. Oh SH, Finones RR, Daraio C, Chen LH, Jin S (2005) Growth of nano-scale hydroxyapatite using chemically treated titanium oxide nanotubes. *Biomaterials* 26(24):4938–4943.
6. Popat KC, *et al.* (2006) Osteogenic differentiation of marrow stromal cells cultured on nanoporous alumina surfaces. *J Biomed Mater Res A* 80(4):955–964.
7. Dalby MJ, *et al.* (2007) The control of human mesenchymal cell differentiation using nanoscale symmetry and disorder. *Nat Mater* 6(12):997–1003.
8. Dalby MJ, *et al.* (2006) Osteoprogenitor response to semi-ordered and random nanotopographies. *Biomaterials* 27(15):2980–2987.
9. Ruiz SA, Chen CS (2008) Emergence of patterned stem cell differentiation within multicellular structures. *Stem Cells* 26(11):2921–2927.
10. La Flamme KE, *et al.* (2007) Biocompatibility of nanoporous alumina membranes for immunoisolation. *Biomaterials* 28(16):2638–2645.
11. Linder L, Carlsson A, Marsal L, Bjursten LM, Branemark PI (1988) Clinical aspects of osseointegration in joint replacement. *J Bone Joint Surg* 70(B):550–555.
12. Puleo DA, Holleran LA, Doremus RH, Bizios R (1991) Osteoblast response to orthopedic implant materials in vivo. *J Biomed Mater Res A* 25:711–723.
13. Mor GK, Varghese OK, Paulose M, Shankar K, Grimes CA (2006) A review of highly ordered, vertically oriented TiO2 nanotube arrays: Fabrication, material properties, and solar energy applications. *Solar Energy Mater Solar Cells* 90:2011–2075.
14. Zhu K, Neale NR, Miedaner A, Frank AJ (2007) Enhanced charge-collection efficiencies and light scattering in dye-sensitized solar cells using oriented TiO2 nanotubes arrays. *Nano Lett* 7(1):69–74.
15. Shankar K, Mor GK, Prakasam HE, Varghese OK, Grimes CA (2007) Self-assembled hybrid polymer-TiO2 nanotube array heterojunction solar cells. *Langmuir* 23(24):12445–12449.
16. Kislyuk VV, Dimitriev OP (2008) Nanorods and nanotubes for solar cells. *J Nanosci Nanotechnol* 8(1):131–148.
17. Albu SP, Ghicov A, Macak JM, Hahn R, Schmuki P (2007) Self-organized, free-standing TiO2 nanotube membrane for flow-through photocatalytic applications. *Nano Lett* 7(5):1286–1289.
18. Jia Y, *et al.* (2007) Synthesis and characterization of TiO2 nanotube/hydroquinone hybrid structure. *J Nanosci Nanotechnol* 7(2):458–462.
19. Su H, Dong Q, Han J, Zhang D, Guo Q (2008) Biogenic synthesis and photocatalysis of Pd-PdO nanoclusters reinforced hierarchical TiO2 films with interwoven and tubular conformations. *Biomacromolecules* 9(2):499–504.
20. Paulose M, *et al.* (2006) Anodic growth of highly ordered TiO2 nanotube arrays to 134 microm in length. *J Phys Chem B* 110(33):16179–16184.
21. Liu S, Chen A (2005) Coadsorption of horseradish peroxidase with thionine on TiO2 nanotubes for biosensing. *Langmuir* 21(18):8409–8413.
22. Varghese OK, Grimes CA (2003) Metal oxide nanoarchitectures for environmental sensing. *J Nanosci Nanotechnol* 3(4):277–293.
23. Park J, Bauer S, von der Mark K, Schmuki P (2007) Nanosize and vitality: TiO2 nanotube diameter directs cell fate. *Nano Lett* 7(6):1686–1691.
24. Oh S, *et al.* (2006) Significantly accelerated osteoblast cell growth on aligned TiO2 nanotubes. *J Biomed Mater Res A* 78(1):97–103.
25. Brammer KS, Oh S, Gallagher JO, Jin S (2008) Enhanced cellular mobility guided by TiO2 nanotube surfaces. *Nano Lett* 8(3):786–793.
26. Aguirre KM, McCormick RJ, Schwarzbauer JE (1994) Fibronectin self-association is mediated by complementary sites within the amino-terminal one-third of the molecule. *J Biol Chem* 269:27863–27868.
27. Pittenger MF, *et al.* (1999) Multilineage potential of adult human mesenchymal stem cells. *Science* 284(5411):143–147.
28. McBeath R, Pirone DM, Nelson CM, Bhadriraju K, Chen CS (2004) Cell shape, cytoskeletal tension, and RhoA regulate stem cell lineage commitment. *Dev Cell* 6(4):483–495.
29. Yamamoto K, *et al.* (2005) Fluid shear stress induces differentiation of Flk-1-positive embryonic stem cells into vascular endothelial cells in vitro. *Am J Physiol* 288(4):H1915–H1924.
30. Saretzki G, *et al.* (2008) Downregulation of multiple stress defense mechanisms during differentiation of human embryonic stem cells. *Stem Cells* 26(2):455–464.
31. Altman GH, *et al.* (2002) Cell differentiation by mechanical stress. *FASEB J* 16(2):270–272.
32. Engler AJ, Sen S, Sweeney HL, Discher DE (2006) Matrix elasticity directs stem cell lineage specification. *Cell* 126:677–689.
33. Norgaard R, Kassem M, Rattan SI (2006) Heat shock-induced enhancement of osteoblastic differentiation of hTERT-immortalized mesenchymal stem cells. *Ann N Y Acad Sci* 1067:443–447.
34. Benoit DS, Durney AR, Anseth KS (2007) The effect of heparin-functionalized PEG hydrogels on three-dimensional human mesenchymal stem cell osteogenic differentiation. *Biomaterials* 28(1):66–77.
35. Mirmalek-Sani SH, *et al.* (2006) Characterization and multipotentiality of human fetal femur-derived cells: Implications for skeletal tissue regeneration. *Stem Cells* 24(4):1042–1053.

Supporting Information

Oh *et al.* 10.1073/pnas.0813200106

SI Materials and Methods

Cell Counting and Viability Test. A coulter particle counter (Beckman Coulter; Z-1 model) was used to count the hMSCs for maintenance and experimental plating densities. To measure live cell elongation at various time points, a fluorescein diacetate (FDA; Sigma) staining was conducted. Cells were plated onto the specimen at a density of 1×10^4 cells per mL. At 2 and 24 h after plating, the cells on the substrate of the specimen were washed by 1× PBS, stained by FDA in PBS (10 μL/10 mL), incubated for ≈30 s, and washed once more.

Immunofluorescence of Fibronectin. After 2 h of incubation in cell culture media or control H_2O with out the presence of cells, Ti and TiO_2 nanotube substrates were fixed in 4% paraformaldehyde in 1× PBS for 15 min at room temperature. Once fixed, substrates were washed twice with 1× wash buffer (1× PBS containing 0.05% Tween-20). Then the samples were incubated for 1 h at room temperature in 5% gelatin (Sigma, from fish skin)/1× PBS followed by the addition of primary anti-BSA antibody (1:100, 2A3E6, Santa Cruz Biotechnology)/anti-bovine serum fibronectin antibody (1:1,000; Primary antibody for staining fibronectin was R457 rabbit polyclonal anti-rat antiserum against the amino-terminal 70-kDa fragment of fibronectin). The samples were incubated overnight at 4 °C. After incubation, substrates were washed three times for 5 min each wash with 1× wash buffer. Goat anti-mouse IgG-FITC (1:1,000, Santa Cruz Biotechnology) and goat anti-rabbit IgG Alexa Fluor 594 (1:1,000, Invitrogen) in 1× PBS was added for double staining and the substrates were incubated again for 1 h at room temperature. After incubation, substrates were washed 3 times for 5 min each wash with 1× wash buffer. The samples were then inverted onto coverslips, mounted, visualized, and photographed by an epifluorescence microscope (DM IRB, Leica Microsystems).

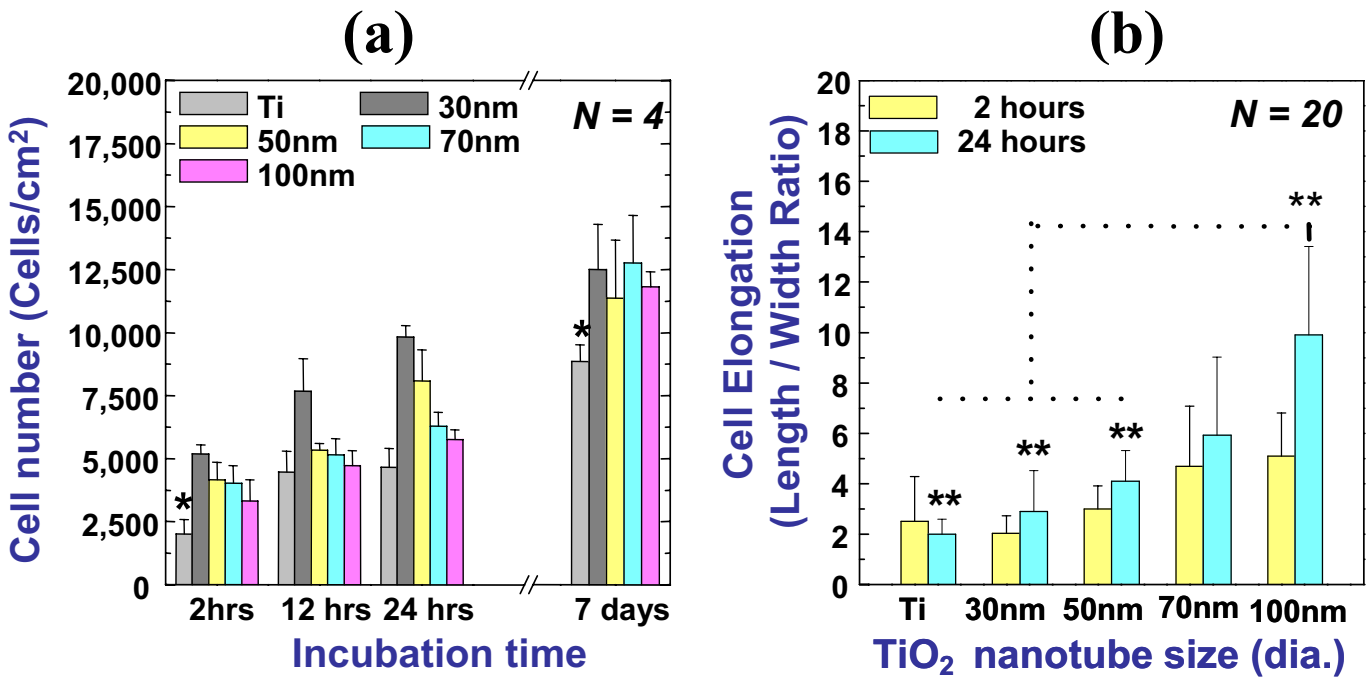

Fig. S1. hMSC behavior on Ti and nanotube substrates. (*a*) Cell number vs. incubation time for various TiO_2 nanotube diameters. (*b*) Cell elongation vs. TiO_2 nanotube diameter at 2 and 24 h. (*c*) Schematic illustration of the overall trend of nano cue effect on hMSC control, for example, after 24 h culture. *, Significant statistical difference between Ti vs. TiO_2 nanotubes ($P < 0.01$); **, significant difference between Ti, 30-, 50-nm nanotube vs. 100-nm nanotube ($P < 0.01$).

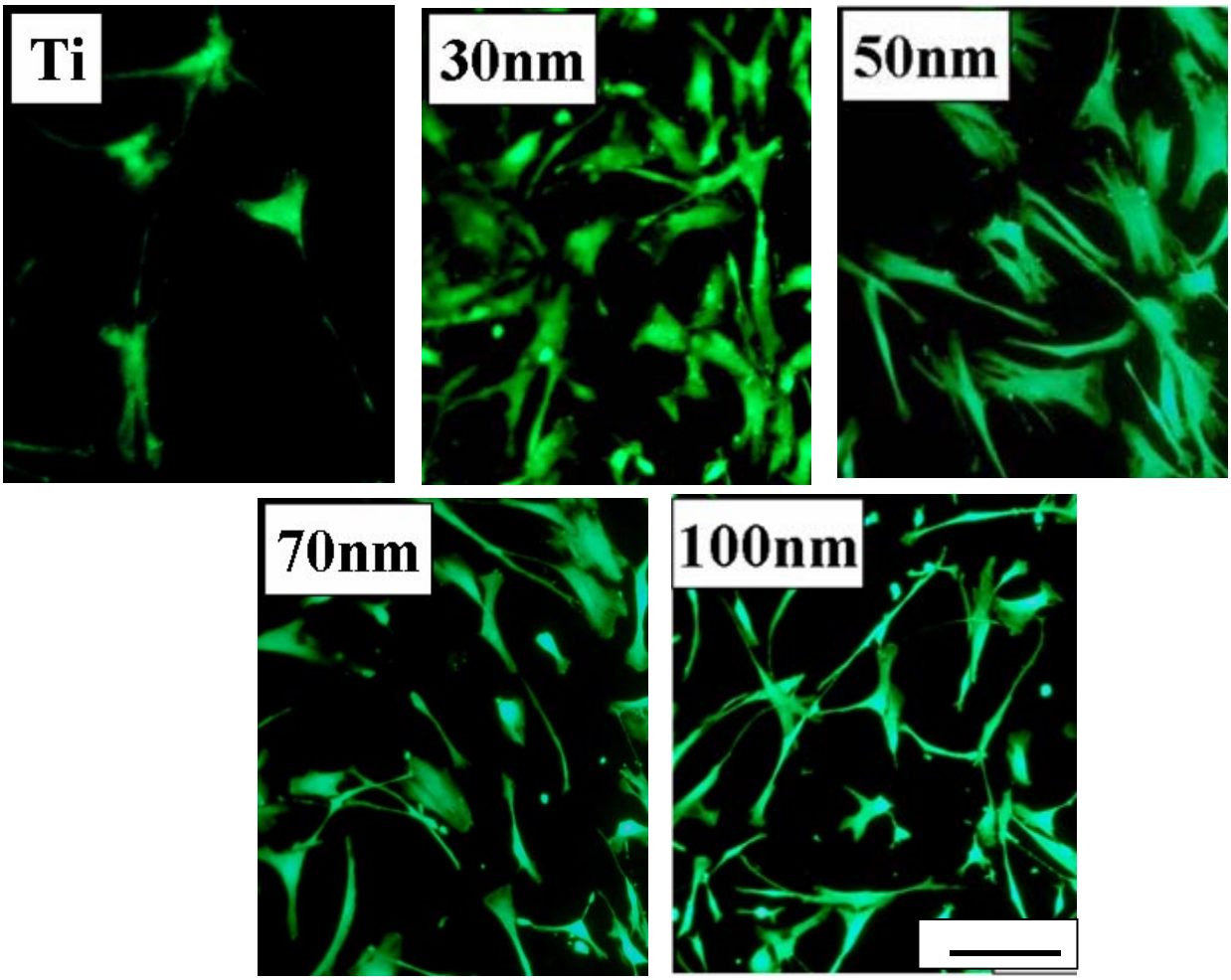

Fig. S2. Fluorescein diacetate (FDA) images of human mesenchymal stem cells (hMSCs) on flat Ti and 30-, 50-, 70-, and 100-nm diameter TiO_2 nanotube surfaces after 24 h of culture. (Scale bar, 100 μm.)

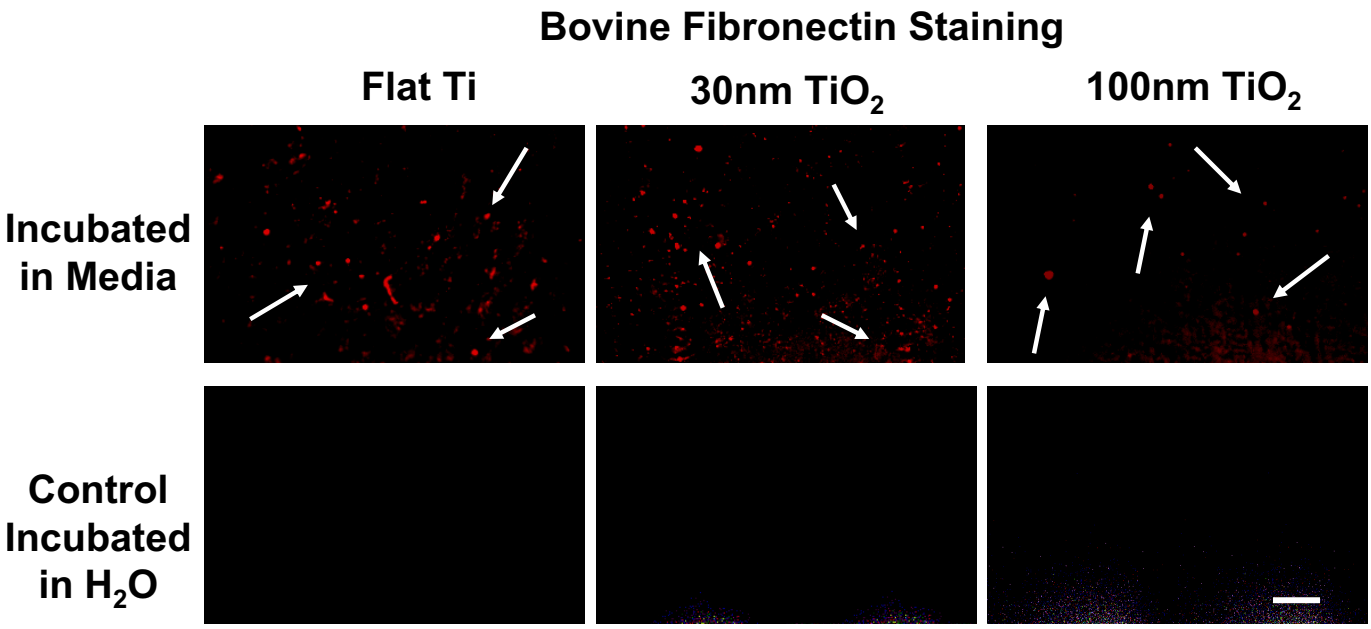

Fig. S3. Bovine fibronectin immunofluorescent staining (red) was performed on flat Ti, 30-nm, and 100-nm TiO_2 surfaces to identify the protein particles on the surface. Fibronectin particles were detected on all surfaces that were incubated in media for 2 h. No fibronectin was detected on control surfaces incubated for 2 h in H_2O. (Scale bar, 20 μm.)